

See discussions, stats, and author profiles for this publication at: <https://www.researchgate.net/publication/51660284>

Nitryl Chloride (ClNO₂): UV/Vis Absorption Spectrum between 210 and 296 K and O(³P) Quantum Yield at 193 and 248 nm

ARTICLE in THE JOURNAL OF PHYSICAL CHEMISTRY A · SEPTEMBER 2011

Impact Factor: 2.69 · DOI: 10.1021/jp207389y · Source: PubMed

CITATIONS

14

READS

98

5 AUTHORS, INCLUDING:



Buddhadeb Ghosh

Phillips 66 Company

8 PUBLICATIONS 53 CITATIONS

SEE PROFILE



Dimitrios Papanastasiou

Foundation for Research and Technology - H...

22 PUBLICATIONS 136 CITATIONS

SEE PROFILE



Ranajit K Talukdar

National Oceanic and Atmospheric Administr...

104 PUBLICATIONS 2,747 CITATIONS

SEE PROFILE



J. M. Roberts

National Oceanic and Atmospheric Administr...

232 PUBLICATIONS 7,013 CITATIONS


SEE PROFILE

Nitryl Chloride (ClNO₂): UV/Vis Absorption Spectrum between 210 and 296 K and O(³P) Quantum Yield at 193 and 248 nm

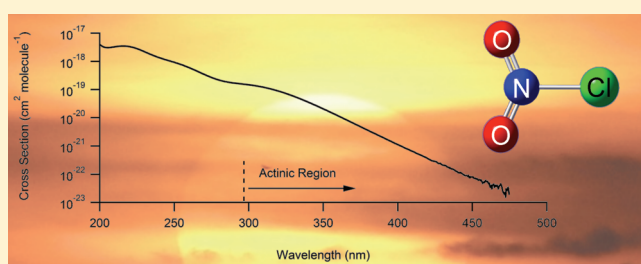
Buddhadeb Ghosh,^{†,‡} Dimitrios K. Papanastasiou,^{†,‡} Ranajit K. Talukdar,^{†,‡} James M. Roberts,[†] and James B. Burkholder^{*,†}

[†]Earth System Research Laboratory, Chemical Sciences Division, National Oceanic and Atmospheric Administration, Boulder, Colorado 80305, United States

[‡]Cooperative Institute for Research in Environmental Sciences, University of Colorado, Boulder, Colorado 80309, United States

 Supporting Information

ABSTRACT: Recent studies have shown that the UV/vis photolysis of nitryl chloride (ClNO₂) can be a major source of reactive chlorine in the troposphere. The present work reports measurements of the ClNO₂ absorption spectrum and its temperature dependence between 210 and 296 K over the wavelength range 200–475 nm using diode array spectroscopy. The room temperature spectrum obtained in this work was found to be in good agreement with the results from Ganske et al. (J. Geophys. Res. 1992, 97, 7651) over the wavelength range common to both studies (200–370 nm) but differs systematically from the currently recommended spectrum for use in atmospheric models. The present results lead to a decrease in the calculated atmospheric ClNO₂ photolysis rate by ~30%. Including the temperature dependence of the ClNO₂ spectrum decreases the calculated atmospheric photolysis rate at lower temperatures (higher altitudes) even further. A parametrization of the wavelength and temperature dependence of the ClNO₂ spectrum is presented. O(³P) quantum yields, $\Phi_{\text{ClNO}_2}^{\text{O}(\text{P})}$, in the photolysis of ClNO₂ at 193 and 248 nm were measured at 296 K using pulsed laser photolysis combined with atomic resonance fluorescence detection of O(³P) atoms. $\Phi_{\text{ClNO}_2}^{\text{O}(\text{P})}(\lambda)$ was found to be 0.67 ± 0.12 and 0.15 ± 0.03 (2σ error limits, including estimated systematic errors) at 193 and 248 nm, respectively, indicating that multiple dissociation channels are active in the photolysis of ClNO₂ at these wavelengths. The $\Phi_{\text{ClNO}_2}^{\text{O}(\text{P})}(\lambda)$ values obtained in this work are discussed in light of previous ClNO₂ photodissociation studies and the differences are discussed.



1. INTRODUCTION

Nitryl chloride (ClNO₂) has been proposed to be a possible atmospheric trace species that is formed in the atmosphere via both heterogeneous^{1,2} and homogeneous^{3,4} chemical processes. However, it was not until recently that ClNO₂ was observed in the lower-troposphere in both ocean/coastal^{5,6} and mid-continental⁷ regions with abundances as high as several ppb - (parts per billion). ClNO₂ was observed to have a strong diurnal profile due to its buildup during the night and rapid UV/vis photolysis after sunrise. In the troposphere, ClNO₂ is thought to play a role in the initiation of early morning radical chemistry that ultimately leads to the formation of ozone. In the stratosphere, ClNO₂ acts as a temporary reservoir of reactive chlorine, which leads to catalytic ozone destruction.

UV/vis photolysis of ClNO₂



is thought to be its primary loss process in the atmosphere and, thus, the mechanism leading to the activation of reactive chlorine. Other ClNO₂ gas-phase atmospheric loss processes,

such as reaction with Cl atoms⁸ and OH radicals,⁹ are known to be negligible relative to photolysis.

The room temperature UV/vis absorption spectrum of ClNO₂ has been reported in several studies.^{10–13} ClNO₂ in the ground X¹A₁ electronic state is planar with C_{2v} symmetry. The UV/vis spectrum is continuous and consists of a strong band centered near 215 nm that corresponds to a 2¹A₁ ← X¹A₁ transition, $\pi^*(\text{NO}_2) \leftarrow n(\text{Cl})$ type,¹⁴ a weaker band near 300 nm, which is possibly due to a transition to an excited triplet state,¹⁴ and a weak unassigned absorption band(s) that extends into the visible wavelength region. Although the spectra reported to date are in good agreement at wavelengths between 200 and 310 nm, discrepancies exist in the wavelength range most critical for its atmospheric photolysis, i.e., >310 nm. The NASA/JPL¹⁵ kinetic data evaluation recommends an average of the ClNO₂ spectra reported by Illies and Takacs¹³ and Furlan et al.¹¹ for use in

Special Issue: A. R. Ravishankara Festschrift

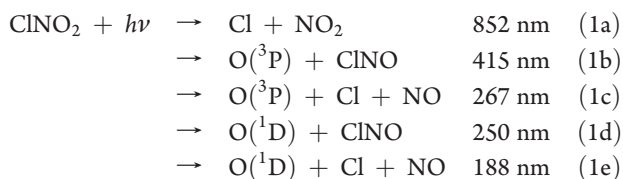
Received: August 2, 2011

Revised: September 7, 2011

Published: September 21, 2011

atmospheric modeling. The IUPAC¹⁶ data panel recommends the ClNO₂ spectrum reported by Ganske et al.,¹² which is substantially weaker in the actinic region. To our knowledge, the temperature dependence of the UV/vis spectrum of ClNO₂ has not been reported to date.

The photodissociation of ClNO₂ in the UV/vis region has several energetically accessible dissociation channels



where NO₂^{*} denotes NO₂ formed in excited electronic states as well as the ground state. The dissociation thresholds given here were calculated for 296 K and ground state species using the thermochemical data from Sander et al.¹⁵ The UV photodissociation of ClNO₂ has been examined in a few studies.^{11,17,18} Nelson and Johnston¹⁷ and Plenge et al.¹⁸ studied the photolysis of ClNO₂ at 350 and 308 nm, respectively, using laser photolysis combined with resonance fluorescence and photoionization mass spectrometry methods, respectively, and concluded that channel 1a was the dominant photodissociation pathway. Plenge et al.¹⁸ also studied the photolysis of ClNO₂ at 240 nm and identified significant yields from channels 1b and 1c, whereas Furlan et al.¹¹ concluded from their laser photolysis-photofragment translational energy spectroscopy experiments that channel 1a was the only significant dissociation channel at 248 nm. Additional studies of the photodissociation channel quantum yields and their wavelength dependence are warranted.

In this work, the photochemistry of ClNO₂ was studied via measurement of its UV/vis absorption spectrum as a function of temperature (210–296 K), i.e., a range relevant to atmospheric photochemistry, and its O(³P) quantum yield at 193 and 248 nm. On the basis of our work, a parametrization of the ClNO₂ UV/vis absorption spectrum and its temperature dependence for use in atmospheric model calculations is presented. Representative atmospheric photolysis rate calculations are presented that illustrate the impact of the present results on the calculated atmospheric photolysis lifetime of ClNO₂. The O(³P) quantum yield in the photolysis of ClNO₂ at 193 and 248 nm was measured using pulsed laser photolysis combined with atomic resonance fluorescence detection of O(³P) atoms to provide further insight into the dynamics of ClNO₂ UV photolysis.

2. EXPERIMENTAL DETAILS

Two independent studies were performed in this work: (1) the ClNO₂ UV/vis absorption spectrum and its temperature dependence were measured using diode array spectroscopy and (2) the O(³P) quantum yield in the photolysis of ClNO₂ at 193 and 248 nm was measured using pulsed laser photolysis combined with atomic resonance fluorescence (PLP-RF) detection of O(³P) atoms. The experimental apparatus and methods used are described separately below.

2.1. ClNO₂ UV/Vis Absorption Spectrum. The ClNO₂ UV/vis absorption spectrum was measured between 200 and 475 nm at 210, 233, 253, 273, and 296 K using diode array spectroscopy with ~1 nm resolution. Absolute absorption cross sections of ClNO₂ at 296 K were not determined in this work, but the

measured spectrum was scaled to its well-established absolute cross section at 216 nm.¹⁵ The ClNO₂ spectra obtained at reduced temperature were scaled relative to the 296 K spectrum using the temperature dependence of the 213.86 (Zn lamp) and 253.65 nm (Hg lamp) cross sections determined in this work.

The experimental apparatus has been used previously in this laboratory and is described in detail elsewhere.^{19,20} The apparatus consists of two absorption cells used to simultaneously measure absorption signals of the ClNO₂ gas-phase sample. The main absorption cell was temperature regulated and had an optical path length of 90.5 cm. This cell was used for the measurement of absorption spectra with a diode array spectrometer. The second absorption cell was operated at room temperature, 296 K, and had a path length of 100.5 cm. This cell was used to measure ClNO₂ absorbance at the Zn and Hg atomic lines using atomic resonance lamp light sources.

Absorption spectra, $A(\lambda)$, were determined using Beer's law

$$A(\lambda) = -\ln\left(\frac{I(\lambda)}{I_0(\lambda)}\right) = L\sigma(\lambda, T)[\text{ClNO}_2] \quad (1)$$

where $I(\lambda)$ and $I_0(\lambda)$ are the measured light source intensity with and without the ClNO₂ sample present in the absorption cell, L is the absorption cell path length, and $\sigma(\lambda, T)$ is the absorption cross section of ClNO₂. The experimental setup for the diode array spectroscopy consisted of two 30 W D₂ light sources and a 0.5 m spectrometer equipped with a 1024 element diode array detector. The wavelength of the diode array spectrometer was calibrated using emission lines from a Hg pen-ray lamp and was accurate to within ±0.1 nm. ClNO₂ was introduced into the absorption cell under both static and flow conditions. $I_0(\lambda)$ was recorded before adding ClNO₂ and after removing it from the absorption cell.

The ClNO₂ absorption spectrum between 200 and 475 nm covers a cross section range of approximately 5 orders of magnitude. Therefore, it was not possible to optimize the determination of the ClNO₂ spectrum over the entire wavelength range in a single absorption measurement. The ClNO₂ spectrum was, therefore, measured in the spectral regions >200 nm (full spectrum), 200–250 nm (using a band-pass filter centered near 215 nm), >280 nm (cutoff filter), and >375 nm (cutoff filter) to optimize the measurements and minimize second-order and scattered light contributions. Spectra were measured using four ClNO₂ concentrations that were approximately (in units of 10¹⁵ molecules cm⁻³) 3, 10, 70, and 100 to optimize the measurement signal-to-noise in the different wavelength regions. The spectra were scaled and combined to produce the overall spectrum between 200 and 475 nm. First, a full spectrum and a spectrum over the wavelength range 200–250 nm was recorded with the same sample using the dual D₂ lamp setup as described elsewhere.^{19,20} The spectra were combined using the common wavelength range 240–260 nm. In a separate measurement, the full spectrum was recorded along with the spectrum recorded with the >280 nm filter, using two higher ClNO₂ concentrations. The spectra were combined using scaling of the spectra in the wavelength range 280–300 nm (lower concentration) and 360–395 nm (higher concentration). Finally, a fourth set of measurements was performed using the >280 and >375 nm filters with the highest ClNO₂ concentration using the 360–390 nm wavelength range to combine the spectra. The overlapping wavelength regions of the spectra agreed to within 2% in all cases.

Absorption spectra at low temperatures were measured while simultaneously monitoring the room temperature absorbance of the sample at 213.86 or 253.65 nm. The second absorption cell used an atomic lamp light source, Zn (213.86 nm) or Hg (253.65 nm) lamp, and a photodiode detector. Band-pass filters (fwhm ~ 15 nm) were used at the entrance and exit of the absorption cell to isolate the atomic lines.

2.2. O(3 P) Quantum Yield. O(3 P) quantum yields were determined relative to that of a well-established reference compound. N $_2$ O and O $_3$ were used as reference compounds in the 193 and 248 nm photolysis experiments, respectively. Quantum yields were determined from the initial O(3 P) atom signals measured in a series of reference-ClNO $_2$ -reference experiments performed over a range of ClNO $_2$ and reference compound concentrations while experimental parameters such as pressure, gas flow rate, laser fluence, and microwave lamp output were kept nearly constant. Experiments performed over a range of concentrations improved the precision of the quantum yield determination and enabled correction for reactant absorption of the resonance fluorescence radiation as described below. The apparatus and experimental procedures have been used in previous studies from this laboratory and are described in greater detail elsewhere.^{19,21–23} All photolysis experiments were performed at room temperature, 296 K.

The photolysis laser power, 0.5 cm 2 beam, was measured at the exit of the reactor with a calibrated power meter. The photolysis laser fluence was varied over the course of the study between 1.2 and 6.8 and 0.5 and 1.1 mJ cm $^{-2}$ pulse $^{-1}$ in the 193 and 248 nm experiments, respectively. A solar blind photomultiplier tube (PMT, 115–200 nm sensitivity) was mounted orthogonal to the microwave lamp and the photolysis laser beam detected the fluorescence signal. The PMT signal was fed into a 100 MHz discriminator-amplifier and then to a digital counting data acquisition board (32 bit, 80 MHz). A 20 W microwave discharge lamp (MgF $_2$ or CaF $_2$ windows) operated with a slow flow of He (~ 0.1 cm 3 s $^{-1}$, STP) at 3 Torr provided the VUV excitation radiation for O(3 P) atom excitation.

O(3 P) temporal profiles were measured using time-resolved atomic resonance fluorescence of the $^3S_1 \leftarrow ^3P_j$ atomic transition at 131 nm. A O(3 P) temporal profile was recorded for each photolysis laser pulse in 20 μ s bins for 40 ms. The signal-to-noise was improved by coadding consecutively measured temporal profiles; 6000 profiles were typically coadded. The background signal, due primarily to scattered light from the microwave discharge lamp, was measured for 1 ms prior to the photolysis laser pulse and subtracted from the O(3 P) temporal profile in the data analysis. The O(3 P) detection limit (S/N = 1) was estimated to be $\sim 1 \times 10^9$ atom cm $^{-3}$ for 1 s integration in a 20 Torr N $_2$ bath gas.

The initial O(3 P) fluorescence signal, S_0 , immediately following the photolysis laser pulse, is proportional to the initial O(3 P) concentration, $[O(^3P)]_0$, which is given by

$$[O(^3P)]_0 = F\sigma_{\text{ClNO}_2}(\lambda, T)\Phi_{\text{ClNO}_2}^O(\lambda)[\text{ClNO}_2] \quad (\text{II})$$

where F is the photolysis laser fluence (photons cm $^{-2}$ pulse $^{-1}$) at the photolysis wavelength λ . An analogous equation also applies for the reference compound. It follows that

$$\Phi_{\text{ClNO}_2}^O(\lambda) = \frac{S_0^{\text{ClNO}_2}}{S_0^{\text{Ref}}} \times \frac{[\text{Ref}]}{[\text{ClNO}_2]} \times \frac{\sigma_{\text{Ref}}(\lambda)}{\sigma_{\text{ClNO}_2}(\lambda)} \times \Phi_{\text{Ref}}^O(\lambda) \quad (\text{III})$$

where S_0 was obtained by extrapolation of the measured pseudo-first-order decay of the O(3 P) atom signal to time zero.

ClNO $_2$ and the reference compounds, O $_3$ and N $_2$ O, attenuate the detected signal by absorbing radiation from the microwave lamp and the O(3 P) fluorescence. Therefore, the O atom sensitivity depends, somewhat, on the reactant concentration and differs for each compound. The experimentally determined S_0 values were corrected to account for the change in sensitivity following the method described elsewhere^{22,24} using the equation

$$\ln\left(\frac{S_0}{B[\text{ClNO}_2]}\right) = Z_{\text{ClNO}_2} + \sigma_{\text{ClNO}_2}(131 \text{ nm})[\text{ClNO}_2]L \quad (\text{IV})$$

where B is the background signal used to scale the fluorescence signal for fluctuations in the lamp intensity and

$$Z_{\text{ClNO}_2} = \ln(P I_0 \sigma_{\text{ClNO}_2}(\lambda, T) \Phi_{\text{ClNO}_2}^O(\lambda)) \quad (\text{V})$$

where P is a proportionality constant, I_0 is the unattenuated microwave lamp intensity, and L is the sum of the pathlengths from the resonance lamp and PMT to the reaction zone. Experiments were performed for a range of $[\text{ClNO}_2]$ and a linear least-squares analysis of $\ln(S_0/B[\text{ClNO}_2])$ vs $[\text{ClNO}_2]$ was used to obtain Z_{ClNO_2} . This analysis was also applied to the reference compound data, and the O(3 P) quantum yield was obtained using

$$\Phi_{\text{ClNO}_2}^O(\lambda) = \Phi_{\text{Ref}}^O(\lambda) \times \frac{\sigma_{\text{Ref}}(\lambda)}{\sigma_{\text{ClNO}_2}(\lambda)} \times \frac{\exp(Z_{\text{ClNO}_2})}{\exp(Z_{\text{Ref}})} \quad (\text{VI})$$

The N $_2$ O and O $_3$ photolysis quantum yield at 193 and 248 nm, respectively, are unity.¹⁵ Under the conditions of the present experiments, O(1 D) atoms produced in the photolysis of O $_3$ and N $_2$ O are collisionally quenched to the ground electronic state in less than ~ 70 ns by the N $_2$ bath gas.¹⁵ The effective O(3 P) quantum yield for O $_3$ and N $_2$ O, $\Phi_{\text{ref}}^O(\lambda)$, in eq VI was, therefore, taken to be unity.

2.3. Materials. He (UHP, 99.999%) and N $_2$ (UHP, 99.99%) were used as supplied. ClNO $_2$ was prepared in the reaction²⁵



The output of an ozone generator was mixed with NO in a slow flow reactor to produce N $_2$ O $_5$, which was collected under vacuum in a Pyrex trap at 195 K. Approximately 0.25 g of HCl was condensed onto a $\times 20$ excess of solid N $_2$ O $_5$ at ~ 77 K. The reaction mixture was then warmed to 195 K and allowed to stand for ~ 10 min. The mixture was recooled to 77 K and another 0.25 g of HCl added. In total, HCl was added to the N $_2$ O $_5$ sample three times. ClNO $_2$ was distilled from the reaction mixture at 195 K and collected in a Pyrex vacuum reservoir trap at ~ 77 K. The ClNO $_2$ sample was stored at 195 K when not in use.

ClNO, NO $_2$, and Cl $_2$ are expected to be the most likely ClNO $_2$ sample impurities. The ClNO gas-phase impurity was evaluated using Fourier transform infrared absorption spectroscopy (FTIR). ClNO was not detectable and was estimated to be $< 0.02\%$. Chemical ionization mass spectrometry (CIMS) was used to evaluate the Cl $_2$ impurity. Cl $_2$ was detected and estimated to be $\leq 0.7\%$. The off-line CIMS measurements provided an approximate estimate of the Cl $_2$ impurity in the samples used in the absorption spectrum experiments, as discussed later. Attempts to measure the Cl $_2$ impurity online during the absorption measurements using CIMS⁶ were unsuccessful because of the high ClNO $_2$ sample concentrations used. NO $_2$ was measured

Table 1. Absorption Cross Sections, 296 K, Used in This Study

wavelength (nm)	cross section ($10^{-20} \text{ cm}^2 \text{ molecule}^{-1}$)		
	N_2O^a	O_3^a	ClNO_2^b
184.95	14.3		
193	8.95		1320 ^c
213.86			345
216			348 ^a
248		1080	96.8
253.65		1148	80.1

^a Cross sections taken from NASA/JPL.¹⁵ ^b ClNO_2 cross sections taken from this study unless noted otherwise. ^c ClNO_2 cross section taken from Furlan et al.¹¹

directly during the course of the UV/vis absorption experiments and found to typically be $\leq 0.05\%$.

ClNO_2 was introduced into the resonance fluorescence apparatus by flowing N_2 bath gas over the liquid sample kept at temperatures between 77 and 195 K. The ClNO_2 concentration was measured online by UV absorption in cells before and after the resonance fluorescence cell. Mixtures of O_3/He (0.2–1%) were prepared manometrically in 12 L Pyrex bulbs. A 5% N_2O (UHP) in He mixture was prepared in a 12 L Pyrex bulb. In the photolysis experiments, the O_3 and ClNO_2 concentrations were monitored before the resonance fluorescence cell by diode array spectroscopy and after the cell at 253.65 nm. The N_2O concentration was measured online after the cell in the 193 nm photolysis experiments at 184.95 nm (Hg lamp). The absorption cross sections used in this study are given in Table 1. Pressures were measured using 100 and 1000 Torr capacitance manometers. Gas flows were measured using calibrated electronic flow meters.

3. RESULTS AND DISCUSSION

The UV/vis absorption spectrum of ClNO_2 was measured at 210, 233, 253, 273, and 296 K over the wavelength range 200–475 nm. The $\text{O}(^3\text{P})$ quantum yield in the photolysis of ClNO_2 was measured at 193 and 248 nm. The results are presented separately below.

3.1. UV/Vis Absorption Spectrum. The UV/vis absorption spectrum of ClNO_2 at 296 K is given in Figure 1. The ClNO_2 absorption cross sections over the wavelength range 200–475 nm are given in the Supporting Information. The weak diffuse vibrational band structure in the wavelength range 220–280 nm that was reported by Miller and Johnston²⁶ and Furlan et al.¹¹ was observed in our spectrum as well. The peak-to-peak cross sections of the structured region are much weaker than the continuum absorption in this region and are more clearly visible after subtracting the continuum component of the spectrum as shown in the Figure 1 inset. The bands are separated by $422\text{--}426 \text{ cm}^{-1}$, which is in good agreement with that reported by Furlan et al.

The ClNO_2 absorption spectrum was measured at low temperature simultaneously with the room temperature absorption at 213.86 and 253.65 nm as described in the Experimental Details. The 213.86 nm cross section at 210 K is greater than the 296 K cross section by 4.8%. The 253.65 nm cross section at 210 K is less than the 296 K cross section by $\sim 11\%$. The experimentally measured cross section ratios at 213.86 and

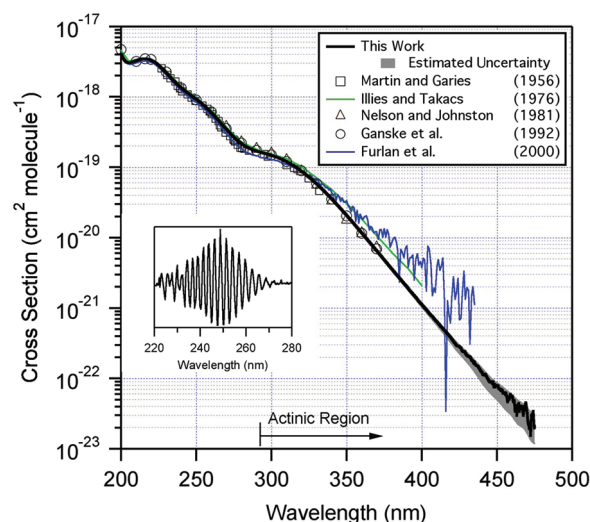


Figure 1. ClNO_2 UV/vis absorption spectrum obtained in this work at 296 K using diode array spectroscopy. The 2σ uncertainty including estimated systematic errors is included as the shaded region. The inset shows the weak diffuse band structure observed in the 220–280 nm region after subtraction of the background continuum. ClNO_2 spectra reported in previous studies, as given in the legend, are included for comparison.

Table 2. ClNO_2 Absorption Cross Section Temperature Dependence Measured Using Diode Array Spectroscopy (σ_{DA}) Relative to Room Temperature, 296 K, Values at 213.86 nm (Zn Line) and 253.65 nm (Hg Line)

temperature (K)	$\sigma_{\text{DA}}(213.86 \text{ nm}, T)$	$\sigma_{\text{DA}}(253.65 \text{ nm}, T)$
	$\sigma_{\text{Zn}}(213.86 \text{ nm}, 296 \text{ K})$	$\sigma_{\text{Hg}}(253.65 \text{ nm}, 296 \text{ K})$
296	1.0 ^a	1.0 ^b
273	1.002 ± 0.00049^c	0.938
253	1.010 ± 0.00068	0.915
233	1.017 ± 0.00044	0.898
210	1.048 ± 0.00053	0.899

^a The ratio measured at 296 K was 0.996 ± 0.004 in two experiments and taken to be 1.0 in the data analysis. ^b A single experiment was performed; the estimated 2σ uncertainty in the ratio was 1.2%. ^c 2σ uncertainty from the precision of the measurement.

253.65 nm for 210, 233, 253, and 273 K are given in Table 2. Test measurements performed with both absorption cells at 296 K yielded a cross section ratio of unity within the precision of the measurements, 0.8%. The cross section ratios obtained at 213.86 and 253.65 nm yielded scaled ClNO_2 spectra that agreed to within the measurement precision, 1%, over the entire wavelength range. An average scaling factor was used in the ClNO_2 spectrum analysis.

The temperature dependence of the ClNO_2 spectrum is shown in Figure 2 where the ratio $\sigma(\lambda, T)/\sigma(\lambda, 296 \text{ K})$ is plotted for wavelengths between 200 and 450 nm. The spectrum at wavelengths $>320 \text{ nm}$ shows a strong temperature dependence, decreasing with decreasing temperature, e.g., $\sigma(400 \text{ nm}, 210 \text{ K})/\sigma(400 \text{ nm}, 296 \text{ K}) = 0.33$. As shown later, the temperature dependence of the absorption spectrum directly impacts the

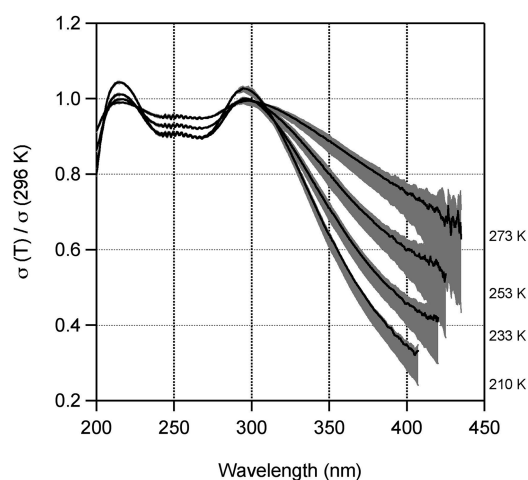


Figure 2. $\sigma(\lambda, T)/\sigma(\lambda, 296 \text{ K})$ ratio of the ClNO_2 spectra measured in this work (solid lines). The shaded regions represent the 2σ (95% confidence) level uncertainty in $\sigma(\lambda, T)$ including estimated systematic errors (see text for details).

calculated ClNO_2 atmospheric photolysis rate. Small systematic increases in the ClNO_2 spectrum were observed near 216 and 296 nm with decreasing temperature. The peaks in the $\sigma(\lambda, T)/\sigma(\lambda, 296 \text{ K})$ ratio near 215, 245, and 290 nm reveal the presence of at least three overlapping electronic transitions between 200 and 450 nm; i.e., the peaks of the transitions show a characteristically weaker temperature dependence.¹⁹ There is also evidence for a contribution from a transition peaking at shorter wavelengths, but outside the wavelength range of our measurements.

The precision of our absorption measurements was high. The $I_0(\lambda)$ spectra recorded before and after measuring $I(\lambda)$ agreed to within 1% at all wavelengths. The ClNO_2 spectra recorded over a range of concentrations obeyed Beer's law. In the 200–400 nm wavelength range, the precision of the measured absorption was $\sim 1\%$. At longer wavelengths, $>400 \text{ nm}$, the uncertainty was greater due primarily to the weaker ClNO_2 absorption; $\sim 3\%$ at 450 nm and $\sim 12\%$ at 475 nm.

A potential source of systematic error in the ClNO_2 spectrum measurement was absorption by sample impurities. The ClNO_2 impurity upper-limit established in the off-line FTIR measurements leads to a negligible contribution to the measured ClNO_2 spectrum at all wavelengths. NO_2 was directly identified in the ClNO_2 sample by its absorption spectrum structure in the wavelength range 430–530 nm. NO_2 was subtracted using reference spectra recorded under identical pressure and temperature conditions. The NO_2 impurity was estimated to be $\sim 0.04\%$. The N_2O_4 , which is present in equilibrium with NO_2



where $K_{\text{eq}} = 5.9 \times 10^{-29} \exp(6643/T) \text{ cm}^3 \text{ molecule}^{-1}$,¹⁵ was calculated to make a negligible contribution to the measured spectrum even at the lowest temperature, 210 K, included in this study. No evidence for HONO absorption¹⁵ was observed under any of the experimental conditions employed in this study.

It was not possible to directly quantify the Cl_2 impurity level in our absorption measurements. An upper limit of the Cl_2 impurity was, however, estimated from the ClNO_2 spectrum measured at 210 K. The upper limit was established by subtracting a Cl_2 reference spectrum, measured under identical conditions, from

the measured spectrum to obtain zero absorbance at 450 nm. This establishes an upper limit for the Cl_2 impurity of $\sim 0.4\%$, i.e., under the assumption that ClNO_2 does not absorb at wavelengths $\geq 450 \text{ nm}$. It is, however, most likely that ClNO_2 does absorb at wavelengths $\geq 450 \text{ nm}$ and that the Cl_2 impurity was actually $<0.4\%$. The ClNO_2 absorption spectra reported in this work were not corrected for a Cl_2 impurity, but the uncertainty due to a possible 0.4% impurity was included in the estimated ClNO_2 cross section uncertainty.

The overall uncertainty in the room temperature ClNO_2 spectrum was estimated to be $<4\%$ between 200 and 300 nm and $<8\%$ in the wavelength range 300–400 nm at the 2σ (95% confidence) level. The uncertainty increases at longer wavelengths primarily due to the uncertainty associated with the Cl_2 contribution to the spectrum. The lower temperature spectra have greater uncertainty at longer wavelengths due to the greater uncertainty in the contribution from Cl_2 . The uncertainty associated with the Cl_2 and NO_2 impurities leads to asymmetric error estimates. The estimated overall uncertainties in the ClNO_2 spectrum are included in Figures 1 and 2.

3.1.1. Comparison with Previous Measurements. Figure 1 includes the ClNO_2 room temperature spectra reported in previous studies for comparison with the present work. The absorption spectra are in good agreement for wavelengths $<310 \text{ nm}$ but deviate significantly at the longer wavelengths. The spectrum measured in this work is in excellent agreement with the spectra reported by Martin and Garies,¹⁰ Ganske et al.,¹² and Nelson and Johnston¹⁷ in the wavelength regions common to these studies, 226–332, 200–370, and 270–370 nm, respectively. Our spectrum is less than reported by Illies and Takacs¹³ and Furlan et al.¹¹ for wavelengths $>320 \text{ nm}$. The deviation from the Furlan et al. spectrum is $\sim 70\%$ at 400 nm, whereas the spectrum reported by Illies and Takacs¹³ is $\sim 45\%$ greater at 400 nm than reported in this work.

We attribute the discrepancies in the reported ClNO_2 spectra to contributions from Cl_2 and to a lesser extent NO_2 impurities in some of the previous studies. The Cl_2 and NO_2 impurities have the greatest impact at the longer wavelengths where the ClNO_2 cross sections are small. Subtracting a $\sim 5\%$ Cl_2 impurity from the ClNO_2 spectra reported by Illies and Takacs¹³ and Furlan et al.¹¹ yields spectra that are in agreement with our spectrum. Subtracting a $\sim 0.25\%$ NO_2 impurity from the Furlan et al. spectrum improves the level of agreement even further. Furlan et al. did not report estimates of Cl_2 or NO_2 impurity levels in their work. Illies and Takacs reported a $\sim 2\%$ $\text{NO}_2/\text{N}_2\text{O}_4$ impurity, but that their ClNO_2 sample contained no detectable, $<2\%$, Cl_2 impurity.¹³ The present results indicate that the Cl_2 impurity was probably underestimated in the Illies and Takacs study.

3.1.2. UV/Vis Spectrum Parameterization. The temperature dependence of the ClNO_2 spectrum was parametrized using an empirical second-order polynomial

$$\sigma(\lambda, T) = \sigma(\lambda, 296 \text{ K}) \times (1 + A_1(\lambda) \times (T - 296) + A_2(\lambda) \times (T - 296)^2) \quad (\text{VII})$$

The $A_1(\lambda)$ and $A_2(\lambda)$ coefficients are provided in the Supporting Information. The fit reproduces the experimental data to within 3% in the 200–400 nm wavelength range and to within $\sim 6\%$ at 450 nm over the temperature range 210–296 K.

The UV/vis absorption spectrum was also fit using the sum of Gaussian functions as was recently applied to the UV/vis absorption spectrum of Cl_2O obtained in this laboratory.¹⁹

The Gaussian fitting provides physical insight into the temperature dependence of the spectrum as well as the wavelength dependence of the photolysis quantum yields, which are described below. The Gaussian fitting also provides a means to empirically compare experimental results with theoretical calculations.¹⁴ A Gaussian function

$$\sigma(\lambda) = \sigma_{\text{Max}} \times \exp \left\{ -W \times \left[\ln \left(\frac{\lambda_{\text{Max}}}{\lambda} \right) \right]^2 \right\} \quad (\text{VIII})$$

represents an electronic transition from the ground state to an excited electronic state where σ_{Max} and λ_{Max} are the cross section and wavelength, respectively, of the transition maximum and W is a term inversely proportional to the width of the absorption band. The sum of five Gaussian functions reproduces the experimental spectrum at each temperature very well, to within 5%.

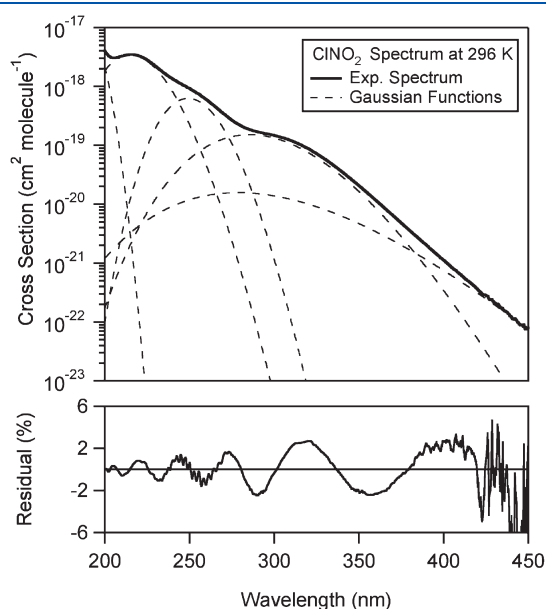


Figure 3. Room temperature ClNO_2 UV/vis absorption spectrum obtained in this work and the simulation using the sum of five Gaussian functions using the parameters given in the Supporting Information, Table S2.

The fit to the 296 K spectrum with Gaussian functions peaking at 190, 215, 249, 279, and 285 nm is shown in Figure 3. The Gaussian fit parameters for the ClNO_2 spectra at each temperature included in this study are given in the Supporting Information.

Although the fits at each temperature are good, it should be noted that the Gaussian parameters show some unexpected temperature dependent behavior. In particular, the fit of the temperature dependence in the long wavelength tail of the spectrum, $\lambda > 350$ nm, requires changes to σ_{Max} , λ_{Max} , and W for the absorption bands centered near 280 and 290 nm. This behavior may be symptomatic of a deficiency of the simple Gaussian fitting approach used to represent the electronic transitions in ClNO_2 . The possible influence of a Cl_2 impurity in the ClNO_2 sample was examined by including its spectrum as a variable parameter in the spectrum analysis. The overall quality of the fit did not improve significantly nor did the Gaussian function temperature dependent behavior change. It was concluded that the presence of a small Cl_2 impurity level is not responsible for the parameter randomness in the fitting of the long wavelength data. Including additional Gaussian functions in the spectrum analysis would possibly improve the overall fit but was judged unjustified.

Lesar et al.¹⁴ used ab initio multireference configuration interaction (MRD-CI) methods to study the electronic absorption spectrum of ClNO_2 . To our knowledge, this is the only theoretical study of the electronic spectrum of ClNO_2 in the literature. Lesar et al. reported vertical excitation energies and oscillator strengths for a number of singlet–singlet transitions. The strongest UV transition, $2^1\text{A}_1 \leftarrow \text{X}^1\text{A}_1$, is centered near 215 nm with an oscillator strength of 0.02. Two weaker transitions near 242 and 281 nm, with oscillator strengths of 0.001 and 4×10^{-5} , respectively, were also reported. The vertical excitation energies of the calculated transitions match reasonably well with the peak positions of the three strongest Gaussian functions, centered at 215, 249, and 279 nm, obtained in our spectrum analysis. However, the relative intensities of the bands are in poor agreement with the theoretical calculations. Lesar et al. also suggested a possible weak triplet transition centered near 300 nm.¹⁴ It is possible that this transition contributes to the long wavelength tail of the ClNO_2 spectrum. Additional theoretical studies of the UV spectrum of ClNO_2 that take into account the present work would be useful.

Table 3. Summary of Experimental Conditions and $\text{O}(^3\text{P})$ Quantum Yields, $\Phi_{\text{ClNO}_2}^{\text{O}}(\lambda)$, Obtained in the 193 and 248 nm Photolysis of ClNO_2 at 296 K

photolysis wavelength (nm)	pressure (Torr, N_2)	photolysis laser fluence ($\text{mJ cm}^{-2} \text{ pulse}^{-1}$)	v^a (cm s^{-1})	$[\text{N}_2\text{O}]$ (10^{14} molecules cm^{-3})	$[\text{O}_3]$ (10^{13} molecules cm^{-3})	$[\text{ClNO}_2]$ (10^{12} molecules cm^{-3})	$\Phi_{\text{ClNO}_2}^{\text{O}}(\lambda)^b$
193	35	5.1	10.7	4.4–26.3		4.5–26.3	0.67 ± 0.07
	24	2.0	16.1	5.7–27.2		10.7–58.6	0.77 ± 0.05
	17	1.2	13.2	10.1–58.6		9.8–50.7	0.69 ± 0.07
	66	6.8	12.0	8.5–40.3		4.1–21.4	0.60 ± 0.06
	18	6.2	13.0	9.5–56.1		5.8–31.4	0.60 ± 0.05
248	18	1.1	9.6		1.4–6.0	4.3–9.8	0.132 ± 0.05
	70	1.1	9.0		1.0–9.8	3.8–12.7	0.143 ± 0.02
	36	0.5	15.2		1.5–8.7	4.2–10.1	0.134 ± 0.01
	36	1.0	15.3		0.9–6.4	1.9–4.7	0.168 ± 0.02
	36	1.0	15.3		1.6–6.1	2.5–5.2	0.152 ± 0.01
	19	1.1	10.1		1.0–7.3	2.7–7.6	0.156 ± 0.01

^a Linear gas flow velocity. ^b The quoted uncertainties are at the 2σ (95% confidence) level from the precision of the measurement.

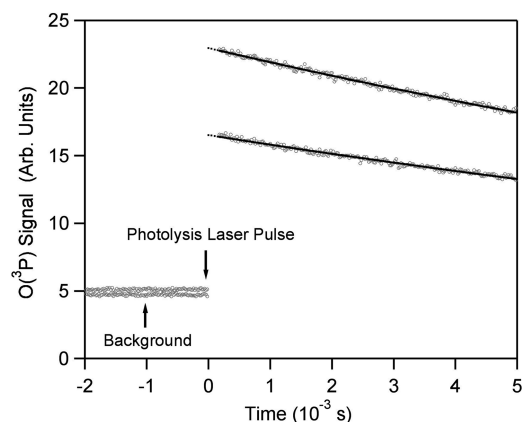


Figure 4. Representative $O(^3P)$ temporal profiles obtained following the 193 nm photolysis of $ClNO_2$; 296 K, 18 Torr N_2 bath gas, photolysis laser fluence of $\sim 7.2 \text{ mJ cm}^{-2} \text{ pulse}^{-1}$, and $ClNO_2$ concentrations of $5.8 \times 10^{12} \text{ molecules cm}^{-3}$ (upper curve) and $1.0 \times 10^{13} \text{ molecules cm}^{-3}$ (lower curve). Pseudo-first-order decay fits of the data to obtain the $O(^3P)$ signal at time zero are shown (solid lines). The dotted lines represent the extrapolation to zero time.

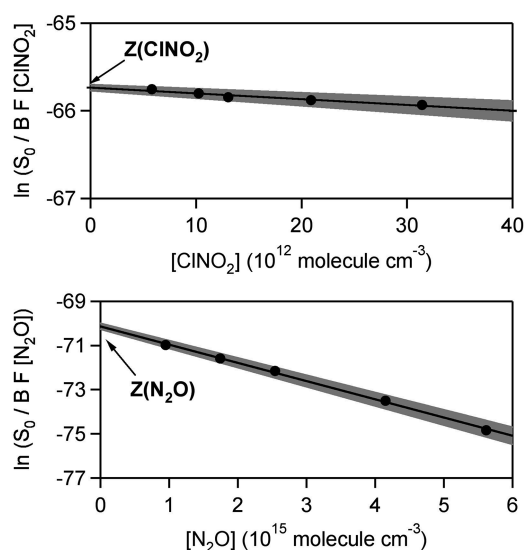


Figure 5. Representative experimental data used to obtain the zero photolyte concentration limiting $O(^3P)$ resonance fluorescence signal for $ClNO_2$ and N_2O in a 193 nm photolysis experiment at 296 K (see text for details). The gray shaded region represents the 2σ uncertainty of the linear least-squares fit.

3.2. $O(^3P)$ Quantum Yield. Table 3 summarizes the experimental conditions and $O(^3P)$ quantum yields in the photolysis of $ClNO_2$ at 193 and 248 nm obtained in this work. Representative $O(^3P)$ atom temporal profiles obtained in the photolysis of $ClNO_2$ at 193 nm are shown in Figure 4. The initial $O(^3P)$ signal, S_0 , was obtained from the $O(^3P)$ temporal profile with a typical 2σ uncertainty of $\sim 1.5\%$. A representative set of S_0 data obtained at different $ClNO_2$ and N_2O concentrations in a 193 nm photolysis experiment are shown in Figure 5. The zero concentration intercept, Z , was obtained from a linear least-squares fit where the typical uncertainty in Z was $<6\%$. The $O(^3P)$ quantum yields at 193 and 248 nm are reported in Table 3 to be 0.67 ± 0.08 and 0.15 ± 0.02 , respectively, where the quoted

uncertainties are at the 2σ level from the precision of the measurements.

The $O(^3P)$ quantum yields were independent of the experimental conditions used including variations in photolysis laser fluence (varied a factor of 5 at 193 nm and a factor of 2 at 248 nm), gas flow velocities (varied a factor of ~ 2), and total pressure (varied between 18 and 70 Torr) to within the precision of the measurements. The overall uncertainty including estimated systematic errors in the $ClNO_2$ and reference compound concentration, absorption cross sections, and the uncertainty in the reference compound quantum yield is estimated to be $\sim 20\%$ at the 2σ (95% confidence) level.

Knowledge of the $O(^3P)$ quantum yield alone does not provide sufficient information to quantify the branching ratios of the $O(^3P)$ producing primary photolysis channels, 1b–1d. It is likely that rapid unimolecular dissociation of NO_2^* , formed in channel 1a, contributes to the measured $O(^3P)$ signal in our experiments. Table 4 provides a summary of the quantum yield and product studies currently available for the photolysis of $ClNO_2$. Nelson and Johnston¹⁷ reported Cl and O atom quantum yields of 0.93 ± 0.15 and <0.02 , respectively, at 350 nm. The O atom observed in their experiments, however, was speculated to have originated from NO_2 photolysis that was present as a 0.15% impurity in their $ClNO_2$ sample.¹⁷ Product studies at 248 and 240 nm have been reported by Furlan et al.¹¹ and Plenge et al.¹⁸ O atom production was not observed in the Furlan et al. study at 248 nm, which does not agree with the present results, leading them to conclude that the sum of channels 1b, 1c, and 1d was $<3\%$.¹¹ Plenge et al. measured Cl^+/O^+ ion intensity ratios using photoionization mass spectroscopy in the 240 nm photolysis of $ClNO_2$, which they interpreted to be due to channels 1a, 1b, and 1c with branching ratios of 0.7, 0.1, and 0.2, respectively.¹⁸ In their analysis it was assumed that $\sim 40\%$ of the NO_2^* produced in channel 1a stepwise dissociated to produce an $O(^3P)$ atom and that the NO_2^* yield in channel 1a was $\sim 70\%$ as reported in previous studies.^{11,27} Their analysis, thus, yields an effective $\Phi_{ClNO_2}^{O(^3P)}$ at 240 nm of ~ 0.5 , which is substantially greater than our measured value of 0.15 at 248 nm. Plenge et al.¹⁸ reported the 308 nm photolysis of $ClNO_2$ branching ratios to be 0.93 and 0.07 for channels 1a and 1b, respectively. That is, a nonzero $O(^3P)$ atom production in the wavelength region relevant to atmospheric photochemistry.

It appears that the results from the beam studies are in stark contrast with the present work, although that may not actually be the case. A significant difference between the Furlan et al.¹¹ and Plenge et al.¹⁸ beam experiments and the present work is the sample temperature. The beam experiments were performed at substantially lower temperatures, although actual vib/rot beam temperatures were not reported. In addition, the difference in the photolysis wavelength between the Plenge et al. study and the present work (240 vs 248 nm) may actually result in excitation to a significantly different excited state distribution leading to different photolysis product branching ratios. For example, our simple Gaussian spectrum analysis presented earlier would predict that excitation at 240 and 248 nm would probe at least two different excited electronic states. Excitation at 248 nm would be $\sim 80\%$ of the transition centered at 250 nm and $\sim 20\%$ of the transition centered at 215 nm, whereas for excitation at 240 nm the distribution would be $\sim 50\%$ and $\sim 50\%$. A greater O atom yield in the transition peaking at 215 nm would, therefore, partially explain the wavelength dependence of the $O(^3P)$ quantum yield. In addition, the low temperature in the beam

Table 4. Summary of ClNO₂ Photolysis Quantum Yield and Product Studies

photolysis wavelength (nm)	experimental method	$\Phi_{\text{ClNO}_2}^{\text{Cl}}(\lambda)$	$\Phi_{\text{ClNO}_2}^{\text{O}}(\lambda)$	intensity ratio $I(\text{Cl}^+)/I(\text{O}^+)$	ref
193	PLP-RF		0.67 ± 0.12		this work
235	REMPI-TOF				Carter et al. ^{27,a}
240	LP-PMS	0.9^b	$0.5^{b,c}$	13.1 ± 1.79	Plenge et al. ¹⁸
248	PLP-RF		0.15 ± 0.03		this work
248	LP-PTES		<0.03		Furlan et al. ¹¹
308	LP-PMS	0.93^b	0.07^b	22.97 ± 3.89	Plenge et al. ¹⁸
350	LFP-RF	0.93 ± 0.15	<0.02		Nelson and Johnston ¹⁷

^a 70% of the NO₂ produced in channel 1a is formed electronically excited, NO₂*. ^b Quantum yields inferred from measured Cl⁺ and O⁺ ion signals.

^c Calculated assuming 40% of NO₂* produced in channel 1a dissociates to O(³P) + NO and that 70% of the NO₂ produced in channel 1a is formed as NO₂*. PLP-RF: pulsed laser photolysis-resonance fluorescence. REMPI-TOF: resonance enhanced multiphoton ionization-time of flight. LFP-RF: laser flash photolysis-resonance fluorescence. LP-PMS: laser photolysis-photoionization mass spectrometry. LP-PTES: laser photolysis-photofragment translational energy spectroscopy.

experiments would result in a narrowing of the absorption bands and possibly even greater differences in the relative proportion, i.e., for 240 nm photolysis there would be even greater excitation to the 215 nm band. The difference in temperature could possibly explain the differences between Furlan et al.,¹¹ $\Phi_{\text{ClNO}_2}^{\text{O}}(248 \text{ nm}) = 0$, and the present work, $\Phi_{\text{ClNO}_2}^{\text{O}}(248 \text{ nm}) = 0.15$. In summary, although the quantum yields and product studies appear to differ significantly there are plausible explanations to reconcile, at least qualitatively, the reported quantum yields and product studies. Detailed theoretical calculations of the ClNO₂ excited state dynamics could possibly provide the information needed to better understand the wavelength and temperature dependence of the O(³P) quantum yield.

To the best of our knowledge, ClNO₂ quantum yield or product studies have not been reported for 193 nm photolysis. The O(³P) atom quantum yield in our work is significant, 0.67, which indicates a strong wavelength dependence in $\Phi_{\text{ClNO}_2}^{\text{O}}(\lambda)$ that is qualitatively consistent with the product yield results from Plenge et al.¹⁸ at 240 nm, our measured quantum yield at 248 nm, as well as the discussion given above.

4. ATMOSPHERIC IMPLICATIONS

ClNO₂ is primarily removed from the troposphere by photolysis at wavelengths greater than 290 nm. Figure 6 shows the wavelength dependence of the ClNO₂ photolysis rate coefficient, $J(\lambda)$, calculated using the spectrum from this work. For comparison, calculations were also performed using the ClNO₂ spectrum currently recommended in NASA/JPL10-6.¹⁵ For this simplified illustrative calculation solar fluxes were obtained using the TUV calculator²⁸ at 40° N, ground level, summer at 6:00 a.m. to simulate sunrise conditions. The wavelengths that contribute most to photolysis fall between 310 and 428 nm (99% of the total photolysis) with a peak in $J(\lambda)$ near 325 nm. The spectrum measured in the present work, therefore, includes the wavelength range most critical to atmospheric photolysis. The integrated $J(\lambda)$ calculated using the room temperature ClNO₂ spectrum obtained in this work is ~30% less than obtained using the NASA/JPL10-6 recommended spectrum. Note that a log–linear extrapolation of the NASA/JPL10-6 spectrum was used to extend the wavelength coverage out to 450 nm, as shown in Figure 6.

Figure 7 shows the integrated photolysis rate coefficient, J , at ground level over the course of the morning. This is important because the ClNO₂ instantaneous photolysis rate coefficient increases steadily throughout the morning as the solar flux

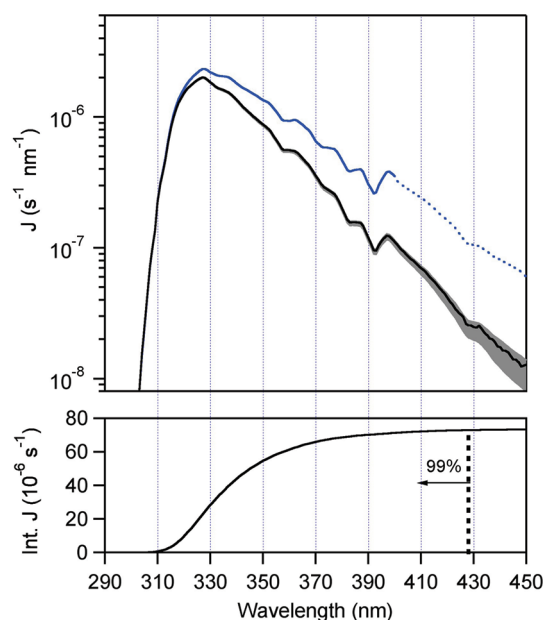


Figure 6. Top frame: ClNO₂ wavelength dependent atmospheric photolysis rate coefficient, $J(\lambda)$, at 0 km altitude, 40° N, July, 6:00 a.m. calculated using the 296 K spectrum obtained in this work with solar fluxes from the TUV calculator.²⁸ The shaded regions represent the range of estimated uncertainty in $J(\lambda)$ due to the uncertainty in the ClNO₂ cross section values. $J(\lambda)$ values calculated using the NASA/JPL10-6¹⁵ recommended ClNO₂ spectrum (296 K) are included for comparison. Bottom frame: Integrated $J(\lambda)$ from frame A.

increases. The effective lifetime of ClNO₂, which is produced during the nighttime, is calculated to be ~2.7 h under these conditions. Therefore, ClNO₂ will act as a radical source throughout the first 3–5 h of morning sunlight and directly impact regional ozone production. This is consistent with the results from recent field observations of ClNO₂.⁷

The temperature dependence of the ClNO₂ spectrum manifests itself in the different cold regions of the atmosphere. For example, the altitude dependence of J is illustrated in Figure 7. Altitude dependent J values were calculated using a standard atmosphere temperature profile²⁹ with the temperature dependent ClNO₂ spectrum from this work. The photolysis rate coefficient in the upper troposphere (lowest temperature region) is approximately a factor of 4 greater than the ground level value due primarily

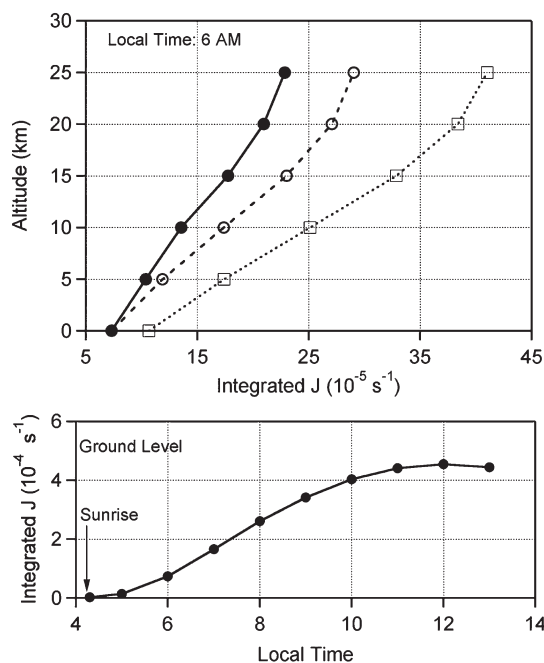


Figure 7. Top frame: Integrated $J(\lambda)$ as a function of altitude calculated for the conditions used in Figure 5 with a standard atmosphere temperature profile and the ClNO_2 spectrum temperature dependence obtained in this study (solid circles). The integrated J calculated using the room temperature spectrum from this study (open circles) as well as from the NASA/JPL10-6¹⁵ evaluation (open squares) are included for comparison. Bottom frame: Integrated $J(\lambda)$ at ground level as a function of local time.

to increasing solar flux with altitude. Including the temperature dependence in the photolysis rate coefficient calculation results in slower photolysis throughout the troposphere and lower stratosphere, e.g., $\sim 15\%$ decrease in the photolysis rate at 15 km.

Figure 7 also includes the ClNO_2 photolysis rate coefficient calculated under the same conditions using the NASA/JPL10-6 room temperature spectrum for comparison. Note that the NASA/JPL¹⁵ recommendation does not include the spectrum temperature dependence, as no experimental data were available at the time. The combination of the ClNO_2 absorption spectrum obtained in this work and its temperature dependence leads to significantly lower photolysis rate coefficients in the UT/LS; e.g., the photolysis rate coefficient at 25 km is $\sim 80\%$ less than calculated using the NASA/JPL10-6¹⁵ recommended room temperature spectrum. Including the results from the current work in model calculations, therefore, significantly impacts the calculated lifetime of ClNO_2 and the release of reactive chlorine throughout the troposphere and stratosphere. The wavelength and temperature dependent ClNO_2 spectrum parametrization provided in the Supporting Information is recommended for use in atmospheric model calculations of ClNO_2 photochemistry.

5. CONCLUSIONS

The ClNO_2 UV/vis absorption spectrum was measured in this work between 200 and 450 nm at temperatures between 210 and 296 K. The results from this work are in good agreement with the 296 K spectra reported previously by Martin and Garies,¹⁰ Ganske et al.,¹² and Nelson and Johnston¹⁷ over the common wavelength ranges. Discrepancies with other previously reported

ClNO_2 spectra were shown to be, most likely, due to the presence of Cl_2 impurities in the previous studies. The ClNO_2 UV/vis absorption spectrum reported in this work leads to longer atmospheric photolysis lifetimes than obtained using the ClNO_2 spectrum currently recommended in the NASA/JPL evaluation.¹⁵ The temperature dependence of the ClNO_2 spectrum leads to an increased atmospheric photolysis lifetime and needs to be included in atmospheric models of tropospheric and stratospheric processes involving ClNO_2 chemistry. The ClNO_2 photolysis lifetime, which is a key parameter in the interpretation of regional tropospheric ozone production, calculated using the data from the present work has a direct impact on calculated early morning radical chemistry in certain locations.^{6,7} This, in turn, directly impacts regional ozone production throughout the day. The wavelength and temperature dependent parametrization of the ClNO_2 absorption spectrum reported in this work is appropriate for use in atmospheric modeling.

■ ASSOCIATED CONTENT

S Supporting Information. Table of ClNO_2 absorption cross section data at 296 K and temperature dependence parametrization. Table of Gaussian function parameters. This material is available free of charge via the Internet at <http://pubs.acs.org>.

■ AUTHOR INFORMATION

Corresponding Author

*E-mail: James.B.Burkholder@noaa.gov.

■ ACKNOWLEDGMENT

This work was supported in part by NOAA's Climate Goal and NASA's Atmospheric Composition Program.

■ REFERENCES

- (1) Finlayson-Pitts, B. J.; Ezell, M. J.; Pitts, J. N. *Nature* **1989**, 337, 241–244.
- (2) Livingston, F. E.; Finlayson-Pitts, B. J. *Geophys. Res. Lett.* **1991**, 18, 17–20.
- (3) Chang, J. S.; Baldwin, A. C.; Golden, D. M. *J. Chem. Phys.* **1979**, 71, 2021–2024.
- (4) Ravishankara, A. R.; Smith, G. J.; Davis, D. D. *Int. J. Chem. Kinet.* **1988**, 20, 811–814.
- (5) Kercher, J. P.; Riedel, T. P.; Thornton, J. A. *Atmos. Meas. Tech.* **2009**, 2, 193–204.
- (6) Osthoff, H. D.; Roberts, J. M.; Ravishankara, A. R.; Williams, E. J.; Lerner, B. M.; Sommariva, R.; Bates, T. S.; Coffman, D.; Quinn, P. K.; Dibb, J. E.; Stark, H.; Burkholder, J. B.; Talukdar, R. K.; Meagher, J.; Fehsenfeld, F. C.; Brown, S. S. *Nat. Geosci.* **2008**, 1, 324–328.
- (7) Thornton, J. A.; Kercher, J. P.; Riedel, T. P.; Wagner, N. L.; Cozic, J.; Holloway, J. S.; Dube, W. P.; Wolfe, G. M.; Quinn, P. K.; Middlebrook, A. M.; Alexander, B.; Brown, S. S. *Nature* **2010**, 464, 271–274.
- (8) Watson, R. T. *J. Phys. Chem. Ref. Data* **1977**, 6, 871–917.
- (9) Ganske, J. A.; Berko, H. N.; Ezell, M. J.; Finlayson-Pitts, B. J. *J. Phys. Chem.* **1992**, 96, 2568–2572.
- (10) Martin, H.; Gareis, R. Z. *Electrochem.* **1956**, 60, 959–964.
- (11) Furlan, A.; Haeberli, M. A.; Huber, J. R. *J. Phys. Chem. A* **2000**, 104, 10392–10397.
- (12) Ganske, J. A.; Berko, H. N.; Finlayson-Pitts, B. J. *J. Geophys. Res.* **1992**, 97, 7651–7656.
- (13) Illies, A. J.; Takacs, G. A. *J. Photochem.* **1976**, 6, 35–42.

- (14) Lesar, A.; Hodoscek, M.; Muhlhauser, M.; Peyerimhoff, S. D. *Chem. Phys. Lett.* **2004**, *383*, 84–88.
- (15) Sander, S. P.; Abbatt, J.; Barker, J. R.; Burkholder, J. B.; Friedl, R. R.; Golden, D. M.; Huie, R. E.; Kolb, C. E.; Kurylo, M. J.; Moortgat, G. K.; Orkin, V. L.; Wine, P. H. *Chemical Kinetics and Photochemical Data for Use in Atmospheric Studies, Evaluation Number 17*; JPL Publication 10-6; Jet Propulsion Laboratory, California Institute of Technology: Pasadena, CA, 2011; <http://jpldataeval.jpl.nasa.gov>.
- (16) Ammann, M.; Atkinson, R.; Cox, R. A.; Crowley, J. N.; Hynes, R. G.; Jenkin, M. E.; Mellouki, W.; Rossi, M. J.; Troe, J.; Wallington, T. J. IUPAC Subcommittee on Gas Kinetic Data Evaluation, 2006; <http://www.iupac-kinetic.ch.cam.ac.uk/>.
- (17) Nelson, H. H.; Johnston, H. S. *J. Phys. Chem.* **1981**, *85*, 3891–3896.
- (18) Plenge, J.; Flesch, R.; Schurmann, M. C.; Ruhl, E. *J. Phys. Chem. A* **2001**, *105*, 4844–4850.
- (19) Papanastasiou, D. K.; Feierabend, K. J.; Burkholder, J. B. *J. Chem. Phys.* **2011**, *134*, 204310.
- (20) Papanastasiou, D. K.; Papadimitriou, V. C.; Fahey, D. W.; Burkholder, J. B. *J. Phys. Chem. A* **2009**, *113*, 13711–13726.
- (21) Dunlea, E. J.; Ravishankara, A. R. *Phys. Chem. Chem. Phys.* **2004**, *6*, 2152–2161.
- (22) Goldfarb, L.; Schmoltner, A. M.; Gilles, M. K.; Burkholder, J. B.; Ravishankara, A. R. *J. Phys. Chem. A* **1997**, *101*, 6658–6666.
- (23) Warren, R. F.; Ravishankara, A. R. *Int. J. Chem. Kinet.* **1993**, *25*, 833–844.
- (24) Talukdar, R. K.; Vaghjiani, G. L.; Ravishankara, A. R. *J. Chem. Phys.* **1992**, *96*, 8194–8201.
- (25) Bernitt, D. L.; Miller, R. H.; Hisatsune, I. C. *Spectrochim. Acta* **1967**, *23A*, 237–248.
- (26) Miller, C. E.; Johnston, H. S. *J. Phys. Chem.* **1993**, *97*, 9924–9933.
- (27) Carter, R. T.; Hallou, A.; Huber, J. R. *Chem. Phys. Lett.* **1999**, *310*, 166–172.
- (28) NCAR Quick TUV Calculator, http://cprm.acd.ucar.edu/Models/TUV/Interactive_TUV/.
- (29) Standard Atmosphere Calculator. In 1976 *Standard Atmosphere Calculator*, <http://www.digitaldutch.com/atmoscalc/>.